Experimental and Computational Studies Indicate Specific Binding of pVHL Protein to Aurora-A Kinase

Imen Ferchichi,[†] Nejla Stambouli,[†] Raja Marrackchi,[†] Yannick Arlot,[‡] Claude Prigent,[‡] Ahmed Fadiel,[§] Kunle Odunsi,[||] Amel Ben Ammar Elgaaied,*[,†] and Adel Hamza*[,†,⊥]

Laboratory of Genetics, Immunology and Human Pathology, Faculty of Sciences of Tunis, Tunisia, UMR 6061 Faculty of Medicine of Rennes 1, France, The Bioinformatics and Computational Biology Initiative, Meharry Medical College, Nashville, Tennessee 36176, and Division of Gynecologic Oncology, Department of Surgical Oncology, Roswell Park Cancer Institute, Buffalo, New York

Received: October 14, 2009; Revised Manuscript Received: November 30, 2009

Overexpression of Aurora-A kinase is commonly detected in many cancers, whereas the von Hippel−Lindau protein (pVHL) is frequently mutated or absent in renal cell carcinoma and is involved in the Ub proteasome complex, an important degradation pathway. In order to establish a link between Aurora-A overexpression and lack of pVHL protein, we hypothesized that pVHL regulates Aurora-A expression through a physical interaction. We present the first evidence, from both biological assays and computational biology techniques, that human pVHL binds strongly to Aurora-A kinase. Extensive molecular modeling, docking, and dynamic simulations demonstrate that the structure of the pVHL protein would allow it to bind to the TPX2 binding region of Aurora-A. In view of Aurora-A's importance as a therapeutic target for the treatment of cancer, this observation provides novel insights into the Aurora-A/pVHL pathway. In addition, the detailed Aurora-A/pVHL binding structure obtained will be valuable for the design of future Aurora-A inhibitors as therapeutic agents.

Introduction

Aurora proteins belong to a small family of serine/threonine kinases that are essential for proliferating cells and have been identified as key regulators of different steps in mitosis and meiosis.[1] The Aurora family of proteins consists of three members, Aurora-A, Aurora-B, and the less well characterized Aurora-C. Human oncogene Aurora-A is located at chromosome 20q13.2, which is commonly amplified in several tumoral tissues.[2,3] The protein structure of the Aurora-A is based on a variable amino terminal regulatory domain, with three putative Aurora boxes (A-box I, II, and III), and a conserved carboxyl terminal catalytic domain, with an activation motif and a destruction box. The Aurora-A serine-threonine kinase plays an important role in cell cycle control, cytokinesis, mitotic entry, centrosome maturation, centrosome separation, spindle assembly, and its maintenance.[4,5] It is also implicated in chromosome segregation and phosphorylates many proteins such as the tumor-suppressor protein p53.[6] Its kinase activity is regulated by phosphorylation, dephosphorylation, and by association with a number of proteins such as TPX2, HEF1, and Bora.[7−9]

The best-known substrate of Aurora-A is TPX2. During mitosis, Aurora-A is activated by autophosphorylation through interaction with TPX2. Hence, TPX2 is considered to be a substrate and an activator of Aurora-A.[7,10] Depletion of Aurora-A by RNA interference delays mitotic entry, and inhibition of Aurora-A with small molecular compounds causes chromosome alignment defects during metaphase, which leads to aneuploidy and cell death overtime.[11,12] Aurora-A is overexpressed and/or amplified in various malignancies such as cancers of the breast, lung, bladder, colorectum, esophagus, ovary, pancreas, and thyroid. Aurora-A is overexpressed in many different tumor types including breast, lung, pancreatic, ovarian, and gastric cancers.[13−19] Although the levels of Aurora-A mRNA are increased in several renal cancer cell lines, the status of Aurora-A in renal cancer remains unclear and warrants further investigation.[20,21]

Among components of the E3 ubiquitin ligase complex involved in Ub-proteasome activity, the von Hippel−Lindau protein (pVHL) appears to be particularly implicated in Aurora-A regulation. Located on chromosome 3p25−26 and including three exons, the VHL tumor suppressor gene is inactivated in hereditary and sporadic carcinomas.[22−24]

The VHL gene encodes the protein pVHL which has three isoforms: isoform 1, pVHL-30 with 213 amino acid residues, is the canonical sequence that is found predominantly in the cytoplasm with less amounts in the nucleus and cell membrane.[25] A shorter form of the protein, pVHL isoform 2, is obtained by alternative splicing, which results in a truncated protein that is missing 39 amino acids (residues 115−154). In many cells, the truncated isoform 2 is the major VHL gene product. Both isoforms (1 and 2) behave very similarly in most biochemical and functional assays performed to date. The pVHL protein isoform 3 is produced by an internal translation initiation at codon 54 of the pVHL-30 mRNA that generates pVHL, which has 160 amino acid residues. This isoform is equally distributed between the nucleus and the cytoplasm but is not membrane-associated.[26]

The pVHL protein is a component of the E3 ubiquitin ligase complex VEC (V, pVHL; E, Elongin E; C, Elongin C) which is implicated in the ubiquitin-proteasome pathway, a major pathway for protein degradation. pVHL has been implicated in

* Corresponding authors. E-mail: ahamz3@email.uky.edu (A.H.).
[†] Faculty of Sciences of Tunis.
[‡] UMR 6061 Faculty of Medicine of Rennes 1.
[§] Meharry Medical College.
[||] Roswell Park Cancer Institute.
[⊥] Present Address: Department of Pharmaceutical Sciences, College of Pharmacy, University of Kentucky, Lexington, KY 40536.

10.1021/jp909869g
Published on Web 01/04/2010

several other cellular functions, including the regulation of cell cycle exit, as well as cell differentiation and growth arrest.[27−29] The pVHL protein also plays a role in the regulation and stability of microtubules.[30−32] This protein is a negative regulator of hypoxia inducible factor (HIF), whose target genes include vascular endothelial growth factor (VEGF) and platelet-derived growth factor (PDGF).[33−35]

Hence, VHL is considered to be a tumor suppressor gene and its inactivation by single mutation, deletion, or hypermethylation is a frequent event in hereditary and sporadic clear cell renal carcinomas (RCC). Several hundred germline mutations in the VHL gene have been reported.[36] Mutations affecting codons 155, 163, and 166 are thought to be involved in the etiology of RCC.[37,38]

Taking into account that the Aurora-A kinase is overexpressed in several cancers and pVHL is inactivated in sporadic and hereditary renal carcinomas, we have addressed the question whether the lack of pVHL protein could lead to Aurora-A expression.

We have addressed the question whether the lack of pVHL protein could lead to Aurora-A overexpression, hypothesizing that normal regulation would take place through an interaction between Aurora-A and pVHL proteins. This hypothesis is supported by the following: (i) Previous results showed that Aurora-A is localized to the pole proximal ends of microtubules and functions as a microtubule organizing center.[39] (ii) pVHL is a microtubule-binding protein and is implicated in the stabilization and orientation of microtubules.[30,32] These observations suggest colocalization of both proteins at the microtubules during mitosis. (iii) pVHL may be involved in the degradation pathway of Aurora-A via the E3 ubiquitine ligase complex. Indeed, a previous study reported that Aurora-A is turned over by the APC ubiquitin-proteasome pathway.[40] Alternatively, pVHL can be phosphorylated by Aurora-A, which possesses serine/threonine kinase activity.

The intent of the present study is to investigate through use of biochemical binding assays and computational studies, the molecular basis of the unusual Aurora-A/pVHL interaction. For this purpose, we obtained preliminary results from biological assays, providing evidence that pVHL binds strongly to Aurora-A. By using computational biology techniques, such as homology modeling, molecular docking, and molecular dynamics (MD) simulation, we explored possible binding modes of the human pVHL protein to the Aurora-A enzyme and identified key residues involved in the protein−protein interaction. The computational effort proposed in the present work first aimed to answer some more detailed structural questions about the interaction of pVHL with Aurora-A, which cannot be answered through experimental studies alone. This work may eventually lead to the design of new inhibitors with enhanced affinity and selectivity for Aurora-A kinase. This study may also help to further elucidate the function of this protein family.

Materials and Methods

Plasmid Construction. Starting from pVHL (von Hippel−Lindau protein isoform 2) Clone I.M.A.G.E (ATCC), we prepared a recombinant plasmid allowing the expression of this protein in fusion with GST (glutathione-*S*-transferase). To obtain full length cDNA of human pVHL, 1 μL of extracted plasmid from VHL Clone I.M.A.G.E was mixed with 25 μL of PCR Master Mix (Promega), 22 μL of nuclease free water, and 1 μL of human VHL-specific primers (Eurogentec). The primers used are listed below, where the underlined nucleotides indicate the recognition sites for the restriction endonucleases BamH1 and EcoR1 (New England BioLabs).

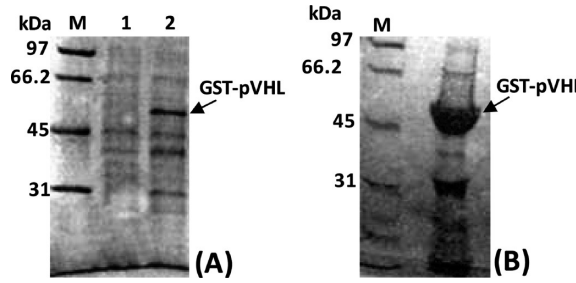

Figure 1. (A) Purification of recombinant human GST-pVHL (SDS polyacrylamide gel stained with Coomassie blue). Lane M: Protein molecular weight markers. Lane 1: Protein extracted from bacteria before addition of IPTG. Lane 2: Protein extracted from bacteria after addition of IPTG. (B) Purification of recombinant human GST-pVHL (SDS polyacrylamide gel stained with Coomassie blue).

Primer sequences used for PCR:

Forward: 5′ GGG-GGA-TCC-CCC-CGG-AGG-GCG-GAG 3′ (BamH1site underlined).

Reverse: 5′ GGG-GAA-TTC-TCA-ATC-TCC-CAT-CCG 3′ (EcroR1site underlined).

The reaction was carried out under the following conditions: an initial step of 5 min at 95 °C, 95 °C for 30 s, 54 °C for 30 s, 72 °C for 1 min 30 s, and 72 °C for 7 min, 30 cycles. The PCR product (650pb) was controlled by agarose gel electrophoresis (1%), with a 1Kb DNA ladder (Fermentas). The fragment was withdrawn and directly ligated into a pGEM-T vector (Promega). All transformants were plated on 2XYT agar plates supplemented with 100 μg/mL ampicillin. Then, we extracted the plasmid pGEM-T-VHL from the clones and the insert was cleaved with BamH1 and EcoR1. The expression vector pGex2TK-USF1 was digested by BamH1 and EcoR1 to release USF1; then, the GST fragment was mixed with the insert containing VHL and was ligated using T4 DNA ligase (Promega) at 16 °C overnight. The ligated product was used to transform *Escherichia* (*E.*) *coli* XL-1 Blue, and extracted plasmids from clones grown in a selective medium were used to transform *E. coli* BL21(DE3)pLysS (Novagen).

Production and Purification of Proteins. We overexpressed and purified two recombinant proteins, GST-pVHL and Hexahistidine Aurora-A ((His)$_6$-Aurora A). Overexpression of GST-pVHL was induced by addition of 1 mM isopropyl β-D-thiogalactopyranoside (IPTG) at 25 °C overnight. (His)$_6$-Aurora A encoded by a pET29 was produced in BL21 and induced by 1 mM IPTG at 25 °C for 3 h. To purify GST-pVHL and GST (control protein), we used glutathione sepharose 4B beads (Amersham Biosciences) and eluted with a buffer containing 10 mM glutathione (10 mM glutathione, 50 mM Tris, pH 8). (His)$_6$-Aurora-A was purified on Ni-NTA agarose (Qiagen) beads and eluted with a buffer containing 250 mM imidazole (IMAC0: 20 mM Tris−HCl, pH 7.5, 500 mM NaCl, 10% glycerin, and 250 mM imidazole). All purification steps were carried out at 4 °C. Induction and purification of the protein were visualized by Coomassie Blue stained SDS-PAGE (Figures 1 and 2). Protein concentrations were determined by Bradford protein assay (Biorad Laboratories) using bovine serum albumin (BSA) as a standard.[41]

GST-Pull-Down Assay. In order to investigate protein−protein interaction between pVHL and Aurora-A, pull-down assays were carried out. Glutathione sepharose 4B beads were blocked with phosphate buffered saline (PBS) 3% bovine serum albumin (BSA) for 1 h at room temperature while being shaken. We

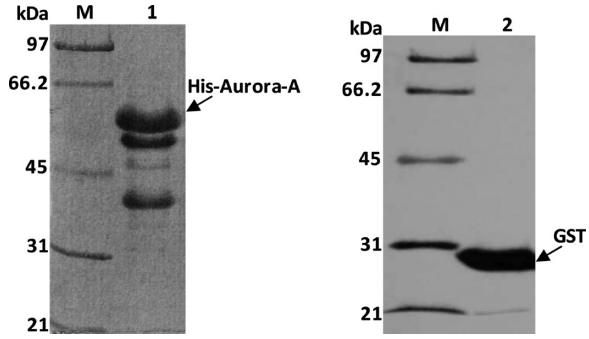

Figure 2. Purification of recombinant human His-Aurora-A (lane 1) and GST (lane 2) (SDS polyacrylamide gel stained with Coomassie blue). Lane M: Protein molecular weight markers.

washed the beads several times and added 250 μg of GST-pVHL (50 μL), 200 μg of GST (50 μL), or 50 μL of elution buffer to 10 μL of beads, and then placed them in a shaking incubator for 1 h at 4 °C. The beads without GST-pVHL were used as a control to detect nonspecific binding. After centrifugation, beads were washed two times with PBS, 250 ng of His-Aurora-A was added, and the beads were placed in a shaking incubator for 1 h at 4 °C. After centrifugation, the beads were washed three times and the proteins were eluted with the addition of 10 μL of Laemmli 2× mercaptoethanol at 95 °C for 5 min. The eluates were analyzed by SDS-PAGE followed by Western blotting.

Hexa-His Pull-Down Assay. To determine if both proteins interact when pVHL is the protein bait or when pVHL is the protein prey, we created a histidine pull-down assay using the two recombinant tagged proteins. A 20 μg portion of Aurora-A was incubated with 40 μg of GST-pVHL (50 μL) or 20 μg of GST (50 μL) in an interaction buffer (50 mM Tris, pH 8, 100 mM KCl, 5 mM $MgCl_2$, 0.1% Triton, 20% glycerol) for 3 h at 4 °C while being shaken. For a negative control, we added 40 μg of GST-pVHL (50 μL) or 20 μG of GST (50 μL) without Aurora-A and incubated under the same conditions. At the same time, beads were blocked with IMAC 5 (IMAC0 and 5 mM imidazole)−3% BSA for 1 h at 4 °C. The resin was washed several times with IMAC 5, and the beads with proteins were mixed for 2 h at 4 °C while being shaken. Then, samples were washed and eluted with 20 μL of IMAC 250 for 10 min at 4 °C. The complexes were separated on a 12% SDS−polyacrylamide gel.

Western Blot. Proteins were separated by 12 or 15% SDS-PAGE, with a lane of SDS-PAGE molecular weight standards (low range, Biorad), and transferred to nitrocellulose (Hybond Amersham). Nonspecific sites on the membranes were blocked in 5% skim milk or BSA in a TBS-T (150 mM NaCl, 20 mM Tris−HCl, pH 7.5, 0.05% Tween 20). We probed with an antibody in 2.5% skim milk or BSA in a TBS-T. The following antibodies were used in this study: monoclonal anti-pVHL (Neomarkers), polyclonal anti-pVHL (Santa Cruz), monoclonal anti-Aurora-A (Sigma), monoclonal anti-Aurora-A produced in the laboratory, and polyclonal anti-GST (Sigma). We further incubated peroxidase-conjugated secondary rabbit or mouse antibodies (Jackson, Interchim) as secondary antibodies. Antibodies were detected by enhanced chemiluminescence ECL (Amersham Pharmacia Biotech) West Pico or West Dura (Pierce).

Homology Modeling of Human pVHL Protein. The amino acid sequence of human von Hippel−Lindau protein isoform 2 (pVHL) (Uniprot: P40337-2) was generated from the GenBank database.[42] The sequence database search was performed by using standard tools, such as blastp and PSI-BLAST to identify the homologue of the known structure from the PDB databank.[43,44] The crystal structure of the human pVHL isoform 1 (pVHL−Elongin C−Elongin B complex) (PDB ID: 1VCB) was used as the template to build the initial pVHL isoform 2 model.[45] Multiple-sequence alignment was performed using the Homology module of InsightII software (Accelrys, Inc.). The 3D model of the human pVHL isoform 2 (denoted by pVHL) was generated by using the automated homology modeling tool at the SWISS-MODEL server.[46,47] Briefly, to generate the core of the model, the backbone atom positions of the template structure are averaged. The template is thereby weighted by its sequence similarity to the target sequence, while significantly deviating atom positions are excluded. The template coordinates cannot be used to model regions of insertions or deletions in the target-template alignment. To generate those parts, an ensemble of fragments compatible with the neighboring stems is constructed using constraint space programming (CSP). The best loop is selected using a scoring scheme, which accounts for force field energy, steric hindrance, and favorable interactions like hydrogen bond formation. If no suitable loop can be identified, the flanking residues are included in the rebuilt fragment to allow for more flexibility. In cases where CSP does not give a satisfying solution and for loops above 10 residues, a loop library derived from experimental structures is searched to find compatible loop fragments. Model construction by the ProModII program included complete backbone and side-chain building, loop building, verification of model quality, including packing, and subsequent energy minimization using the Gromos96 force field.[46−48]

Validation of the Models. In general, every homology model contains errors in the initial structure of the model. The number of errors for a given method is mainly dependent on the percentage of sequence identity between the template and the target and on the number of errors in the template itself. An essential step in the homology modeling process is to verify and/or validate the model. We used several steps to estimate possible errors in our 3D models. The stereochemical quality and energetic parameters of these structures were evaluated to determine whether the bond lengths and bond angles were within their normal ranges, or whether there were lots of bumps in the models (corresponding to a high van der Waals energy). These were evaluated by the Whatcheck, ProsaII, Anolea, and Verify3D analysis reports provided by the SWISS-MODEL server.[49−52] The quality of the final model was determined from the B-score values provided by SWISS-MODEL and the Cα root-mean-square (rms) deviation values between the modeled and template proteins. The models were also analyzed for violations of main chain Phi/Psi dihedral bond angle ratios and backbone/side chain steric conflicts.

Model Refinement. To refine the homology model, the initial pVHL model was solvated in water and subjected to a short run of energy minimization (3000 cycles) to relieve possibly unfavorable steric interactions and to optimize the stereochemistry (see below for MD simulation procedure). This refined 3D model of pVHL was further evaluated periodically for its stereochemical quality, as well as its residue packing and atomic contacts as described above.

Molecular Docking. Docking calculations were performed on the pVHL considered as the "*ligand*" in the Aurora-A binding site using the "*automatic docking*" Affinity module of the InsightII package (Accelrys, Inc.). The Affinity methodology uses a combination of Monte Carlo type and simulated annealing procedures to dock the guest molecule (ligand) to the host (receptor). A key feature is that the "bulk" of the receptor,

defined as atoms not in the binding (active) site specified, is held rigid during the docking process, while the binding site atoms and ligand atoms are allowed to move.

During the initial docking calculation process, a roughly docked Aurora-A/pVHL complex was prepared. Thus, the first step of building the Aurora-A/pVHL complex was to dock the ligand (pVHL) to Aurora-A by virtue of their geometric complementarity. We aimed to find where the ligand could be inserted most comfortably. Currently, there is no resolved structure to provide any atomic details of the interaction of pVHL with Aurora-A. However, the complex structure of Aurora-A with TPX2, in which the secondary structure of the helical segment (residues 30−42) domain is strikingly similar to the α-helix H1 of the pVHL structural model, has been solved.[53] For our study, we built an initial model of the Aurora-A/pVHL complex based on the crystal structure of the TPX2-bound domain (residues 30−42) to Aurora-A active site (PDB code: 1OL5).[53]

Specifically, the docking procedure consists of superimposing the Cα helix H1 of pVHL onto the Cα helix domain of TPX2, followed by replacing the TPX2 ligand in the Aurora-A/TPX2 complex with our pVHL homology model.[53] The initial position of the pVHL-onto-TPX2 structure was followed by successive translation along the *Z*-axis of the TPX2 helix to maximize the overlap between the two helical structures. Thereafter, the other parts of pVHL were positioned in an approximate orientation on the Aurora-A active site to make the appropriate interactions without steric clashes between the ligand and the residues in the side chain of the pocket.

Thus, we obtained a reasonable starting structure for further modeling studies. The Affinity/InsightII module was used to energy-minimize the starting structure. This process was designed to remove bad contacts and poor internal geometry in the initial structure and to obtain a reasonable starting point for subsequent searches. Finally, the binding site was defined as a sphere centered on the initial position of the ligand with an approximately 10 Å radius around the catalytic active site of Aurora-A. The ligand (pVHL) was then moved by a random combination of translational, rotational, and torsional changes. The random movement of the ligand represents both the conformational space of the ligand and its orientation with respect to Aurora-A. This procedure has the advantage of overcoming any energy barrier on the potential energy surface. For each resulting randomly moved structure, the energy was evaluated and compared to that of the previously energy-minimized structure. If the calculated energy change was within the specified (default) energy tolerance parameter, it was considered to have passed this first step and the structure was energy minimized. The second step was for fine-tuning the docking. Whether the final energy-minimized structure was accepted or rejected was based on the Metropolis energy criterion as implemented in the software and its similarity to structures found before. The Metropolis criterion was found to be best suited for finding a very small number of docked structures with very low energies (∼100 lowest-energy minimized structures were kept).

We further refined these Aurora-A/pVHL binding structures with ∼100 ps of MD simulations at $T = 298.15$ K. The energy minimization was performed by using the steepest descent algorithm first until the maximum energy derivative was smaller than 4 kcal/mol/Å and then used the conjugated gradient algorithm until the maximum energy derivative was smaller than 0.001 kcal mol^{-1} $Å^{-1}$.

During the energy minimization and MD simulation, only the ligand (pVHL) and residues of the side chain in the Aurora-A binding pocket were allowed to move freely. The conformational searches (docking poses), energy minimization, and MD simulation for these processes were performed by using the Amber force field implemented in the Discover_3/InsightII calculation engine. The nonbonded interaction cutoff and the dielectric constant were set up to group based (20 Å cutoff distance) and distance dependent ($\varepsilon = 4r$) to mimic the solvent environment, respectively.[54,55] The MD simulation was performed with a time step of 1 fs.

Cluster Analysis. The docked structures were examined, and the most favored cluster in the distribution of ligand (pVHL) poses was identified using a method similar to that previously described.[56,57] Briefly, for every docked pose, the number of ligand neighbors within a threshold root mean squared deviation (rmsd) was determined. The pose with the most populated cluster was identified as the most favored pose or conformation. For the studied pVHL ligand, each docked pose was clustered by 2.0 Å of rmsd criterions. Single conformations or poses disconnected from the rest of the ensemble were considered as unlikely conformations and hence were identified and removed.

After the initial criterion was satisfied, the second step was an examination of the different interactions that could be formed between the Aurora-A enzyme and the helix H1 structure of pVHL ligand. In this way, the best cluster was selected on the basis of the following criteria: lowest interaction energy (sum of the electrostatic and van der Waals interaction energy terms) of the Aurora-A/pVHL complex, hydrophobic interaction formed between the concave active site of Aurora-A and the Leu117 side chain of the pVHL ligand. Finally, the ligand conformation from the best cluster with the lowest interaction energy was subjected to energy minimizations and MD simulations on the explicitly solvated protein−protein complex (see below for the MD simulations) that can better account for the solvent effects on the protein−protein binding.

Molecular Dynamics Simulation. The MD simulations were performed by using the GROMACS 3.0 software package, with a united atom version of the GROMOS96 force field, similar to our previous study of other protein−ligand systems.[58−62] The lysines, arginines, and N-terminal amine groups were put in the protonated state with a charge of +1. The carboxyl groups of aspartic and glutamic acids and of the C-terminal residue were deprotonated and charged negatively.

The initial geometry of the Aurora-A/pVHL structure was neutralized by adding appropriate sodium counterions and was solvated in a rectangular box of SPC water molecules with a minimum solute−wall distance of 10 Å.[63] Prior to MD simulations, the protein was kept fixed with a constraint of 500 kcal $mol^{-1}Å^{-2}$, and we energy-minimized the positions of the water molecules. Then, the entire solvated system was fully energy-minimized without any constraints. The MD simulation was run by using the energy-minimized structure as the starting structure, and the particle mesh Ewald (PME) algorithm was used for dealing with long-range interactions.[64] Each of the solvated systems was carefully equilibrated before a sufficiently long MD simulation at room temperature. The MD simulations were performed with a periodic boundary condition in the NPT ensemble using a Berendsen barostat with a pressure (P) of 1 bar and a Berendsen thermostat at a reference temperature (T) of 298.15 K.[65] The time step of the simulation was 2.0 fs with a cutoff of 12 Å for the nonbonded interactions, and the LINCS algorithm was employed to keep all bonds involving hydrogen atoms rigid.[66] Constant-volume was carried out for 50 ps, during

	1	2	3	
GST-pVHL	-	+	-	First step
GST	-	-	+	
His-Aurora-A	+	+	+	Second step

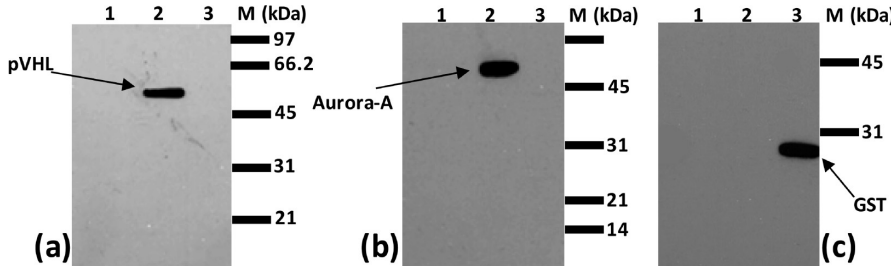

Figure 3. GST-pull-down assay. Binding to glutathione-agarose beads of GST (lane 3), GST-pVHL (lane 2) followed by "*in vitro*" incubation with $(His)_6$-Aurora-A, elution of the bound proteins from the beads, and Western blotting. A negative control consists of direct incubation of $(His)_6$-Aurora-A with beads using at the first step a buffer without any protein (lane 1). Lane M: molecular weight. (a) WB with anti-pVHL antibody detected by enhanced ECL. (b) WB with anti-Aurora-A antibody detected by enhanced ECL. (c) WB with anti-GST antibody detected by enhanced ECL.

which the temperature was raised from 10 to 300 K. Then, a long production run of constant-pressure MD was carried out at 300 K.

The MD simulations on the Aurora-A/pVHL complex were performed with a constraint of 20 kcal mol^{-1} $Å^{-2}$ on the Cα atoms of the Aurora-A enzyme. The atomic coordinates of the simulated structure were saved every 5 ps for analysis. The final structure of the Aurora-A/pVHL complex was obtained as the average of the last 1000 ps of MD minimized until a convergence of 0.05 kcal mol^{-1} $Å^{-1}$. An analysis of the MD trajectory was performed using the GROMACS package.

The pVHL binding free energies (Gibbs free energy: $\Delta G_{bind}{}^{pVHL}$) for the Aurora-A/pVHL complex were estimated using the sietraj program.[67,68] This program calculates ΔG_{bind} for snapshot structures from the MD simulations with a rigid infinite separation of the protein and nucleotide.[67] ΔG_{bind} is the sum of the intermolecular van der Waals and Coulomb interactions, plus the change in reaction field energy (determined by solving the Poisson−Boltzmann equation) and nonpolar solvation energy (proportional to the solvent-accessible surface area).[67] ΔG_{bind} is then scaled by an empirically determined factor, obtained by fitting to a training set of 99 protein−ligand complexes.[67] The scaling can be considered a crude treatment of entropy−enthalpy compensation.

Essential Dynamics. The extraction of the data on the local flexibility of pVHL protein from MD simulations was performed after essential dynamics (ED) analysis. ED analysis is a widely applied technique based on principal component analysis (PCA) of conformational ensembles.[69]

Essential dynamics is a technique that allows the identification of the correlated motions of a protein during a trajectory generated by an MD simulation.[69−71] After removal of the rotational motions, a covariance matrix is constructed. The diagonalization of the matrix leads to a set of eigenvectors/eigenvalues. Each eigenvector represents one single direction in a multidimensional space, whereas the eigenvalue is the amplitude of the motion along the eigenvector. The Cα displacement along each eigenvector can provide insights into the concerted motions of the protein along each direction along with their amplitude. The projection of the displacements on each eigenvector shows the width of the essential space explored by the system as a function of time. Only the Cα atoms were included in the analysis, because it was demonstrated that this reduction of the analysis can retain all of the relevant information needed to separate the essential subspace and identify the important modes in the protein dynamics.[69] The local flexibility of pVHL protein was then reported as the root-mean-square fluctuation (RMSF) on the positions of the Cα atoms as calculated from the coordinate of the system in the essential subspace. The RMSF of the Cα atoms i is a measure of the deviation between its position, r_i, and its time-averaged position: $RMSF(i) = (\langle r_i^2 \rangle - \langle r_i \rangle^2)^{1/2}$, with $\langle\ \rangle$ indicating a time-average.

Results and Discussion

In Vitro Studies. To investigate possible physical interaction between the pVHL and Aurora-A proteins, we used an *"in vitro"* GST-pull-down assay. Bound to glutathione sepharose beads, GST-pVHL was incubated with His-Aurora-A. As a negative control, Aurora-A (prey protein) was incubated with GST alone (bound to beads also) or with beads alone without a bait protein. Those controls were used to exclude any nonspecific binding of Aurora-A to GST or to the beads. Aurora-A fixation to beads carried out by Western blotting was detected only when GST-pVHL was previously fixed to beads (Figure 3b, lane 2), suggesting that there is a specific interaction between both proteins.

To further examine the physical association of the pVHL and Aurora-A proteins, we used *in vitro* histidine-pull-down. His-Aurora-A, conjugated to Ni-NTA agarose beads, was incubated with GST-pVHL. At the same time and under the same conditions, as a first control, we replaced GST-pVHL by GST alone and, as a second control, beads were directly incubated with GST-pVHL. The controls were performed in order to exclude any nonspecific binding to beads of GST-pVHL or GST alone. As shown in Figure 4b, lane 3, GST-pVHL was specifically pulled down by His-Aurora-A. These findings were consistent with the above-mentioned GST-pull-down results.

As observed in lanes 2 and 3 (Figure 4), a nonspecific band of protein was revealed. Since anti-pVHL antibodies are polyclonal, they could cross-react with a bacterial protein that contaminated GST and GST-pVHL recombinant proteins and gave rise to the apparent band in the Western blot. This protein seems to interact with Aurora-A and needs further investigation to be fully characterized.

Homology Modeling of Human pVHL Isoform 2. The physical interaction between pVHL and Aurora-A led us to investigate whether any functional interaction between these two

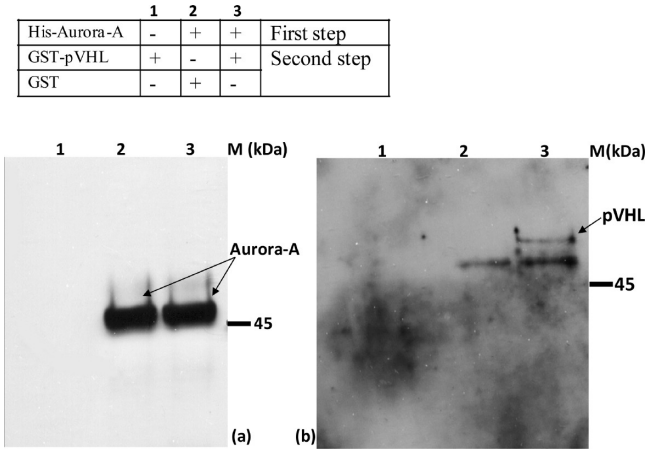

Figure 4. Histidine-pull-down assay. Binding to Ni-NTA agarose beads of $(His)_6$-Aurora-A, followed by "*in vitro*" incubation with GST alone (lane 2) or GST-pVHL (lane 3), elution of the bound proteins from the beads, and Western blotting. A negative control consists of direct incubation of GST-pVHL (lane 1) with beads using at the first step a buffer without any protein. Lane M: molecular weight. (a) WB with anti Aurora-A antibody detected by enhanced ECL. (b) WB with anti-pVHL antibody detected by enhanced ECL.

```
              60         70         80         90        100        110
P40337-2 MEAGRPR PVLRSVNSRE PSQVIFCNRS PRVVLPVWLN FDGEPQPYPT LPPGTGRRIH
P40337-1 MEAGRPR PVLRSVNSRE PSQVIFCNRS PRVVLPVWLN FDGEPQPYPT LPPGTGRRIH
        ←---------------------------- β-domain ----------------------
       120        130        140        150        160        170
SYR                                                VYTLKE RCLQVVRSLV KPEN
SYRGHLWLFR DAGTHDGLLV NQTELFVPSL NVDGQPIFAN ITLPVYTLKE RCLQVVRSLV KPEN
-----------------------------------------→        ←------- α-domain--
              190        200        210
YRRLDI VRSLYEDLED HPNVQKDLER LTQERIAHQR MGD
YRRLDI VRSLYEDLED HPNVQKDLER LTQERIAHQR MGD
-------------→  ←---- β-domain→
```

Figure 5. Sequence alignment of human pVHL isoform-2 (AC: P40337-2) with isoform-1 (AC: P40337-1) (PDB ID: 1VCB). α-helices are indicated in bold residues.

proteins occurs. For this purpose, we first built the pVHL isoform 2 protein by homology using the high-resolution X-ray crystal structure of pVHL isoform 1 bound with Elongin C−Elongin B as the template (PDB ID: 1VCB).[45] The amino acid sequence alignment revealed ∼74% identity between the human pVHL isoform 1 and isoform 2. As shown in Figure 5, the only difference between these two pVHL isoform sequences is the missing residues 114−154 in the sequence of pVHL isoform 2.

The detailed homology modeling procedure has been discussed in the Materials and Methods section. Energy minimization of pVHL helped relieve any steric clashes or improper geometries in the protein structure to produce a model with correct bond lengths and bond angles and where individual atoms were not too close together. To investigate the quality of the refined pVHL model structure, a variety of computational tests (described above) were performed. In summary, the quality of the pVHL model was checked by using three different types of criteria. The results showed that the backbone conformation (Procheck), the residue interaction (Prosa-II), and the residue contact (Whatif) are all well within the ranges established for a reliable protein structure. After analyzing the validation results, we came to the conclusion that we obtained a 3D model of pVHL isoform 2 sufficient to characterize its binding site and to explore pVHL binding with the Aurora-A enzyme. The refined structure of the homology model of pVHL is shown in Figure SI-1 in the Supporting Information.

Computational Docking of Human pVHL Model to Aurora-A Enzyme. Biochemical studies revealed that pVHL protein forms a complex with Elongin B−Elongin C, Rbx1, and Cul2.[72] This complex possesses ubiquitin ligase activity and targets the α-subunits of the heterodimeric transcription factor hypoxia-inducible factor (HIF) for proteasomal degradation when oxygen is available.[72] Interestingly, pVHL contains two mutational hotspot regions called the alpha and beta domain. The α-domain binds directly to Elongin C and nucleates the formation of the complex, while the β-domain is a substrate docking site and binds directly to HIFa family members (HIF1α, HIF2α, and HIF3α).[45,73]

At present, it is well-known that the binding of pVHL with the Elongin C and Elongin B proteins involves the residues of the α-domain moiety. The α-domain of pVHL (residues 155−192 in isoform 1 and residues 114−154 in isoform 2) consists of three α-helices (H1, H2, and H3). These pack in an arrangement reminiscent of a four-helix cluster ("*folded leaf*" classification), except for the absence of a fourth VHL helix. A helix from Elongin C fits into this gap and completes the four-helix cluster arrangement, resulting in two pairs of helices packing at a perpendicular angle (PDB ID: 1VCB).[45] The concave pVHL binding surface is dominated by hydrophobic residues, and sequence alignment indicates that this surface hydrophobicity is likely conserved in fly and yeast Elongin C orthologs.[45] The pVHL−Elongin C interface is almost completely hydrophobic with only a handful of significant hydrogen bonds at the periphery.

To complement our experimental work on Aurora-A/pVHL binding, we investigated the interaction between these two proteins by carrying out molecular modeling studies. In these studies, we docked and MD-simulated a large number of potential binding modes of the pVHL homology model to the human Aurora-A enzyme, representing a wide range of flexibility available to the pVHL molecule. We have assumed, in the absence of any experimental data to the contrary, that the Aurora-A enzyme itself retains the same fold as that in the native crystal structure.

Visual inspection of the solvent-accessible surface area of the Aurora-A crystal structure revealed the presence of a hydrophobic crevice located at the interface between two helices (residues 174−189 and 231−251), in which residues 30−42 of the TPX2 molecule interact.[53] The structural homology between pVHL and the relevant peptide (residues 1−43) of the TPX2 protein is not strong enough to allow a reliable superimposition, which would have provided an indication about the localization of a putative pVHL binding site. Nonetheless, α-helix H1 (residues Leu117−Leu128) of pVHL and the helical conformation of residues Asn30−Leu41 of TPX2 can easily be compared and superimposed (Figure SI-2 in the Supporting Information). Indeed, the residues Leu117−Leu128 of pVHL display the same features that the TPX2 protein uses to bind Aurora-A: (1) a positively charged amino acid defining a positive track suitable for binding the pVHL α-helix H1 to the Aurora-A protein surface; (2) an exposed hydrophobic Leu117 residue (which corresponds to Phe35 in TPX2) providing stacking interactions with the hydrophobic pocket of Aurora-A (Figure SI-2 in the Supporting Information).[53]

To see how the pVHL molecule might anchor in the Aurora-A binding site pocket, we first inserted the pVHL α-helix H1 into the Aurora-A binding cavity and oriented it in a favorable position, thus preventing any steric hindrance with the nearby residues of the pocket. When both motifs (pVHL and TPX2) were superimposed, the canonical binding face observed on the Aurora-A protein of the Aurora-A/TPX2 crystal structure shows a similar buried surface in the Aurora-A/pVHL binding interface. Starting from this initial rough pose, molecular docking using

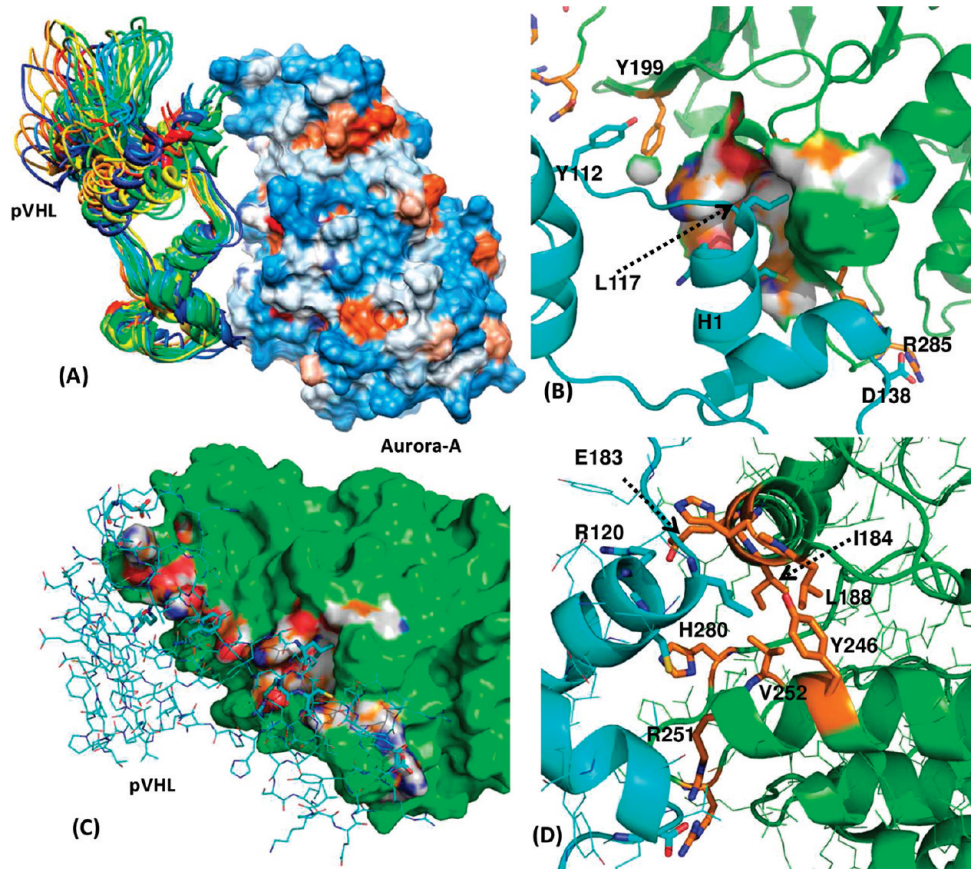

Figure 6. (A) View of the Aurora-A/pVHL complex with the pVHL poses in the most populated cluster. The binding pocket of the Aurora-A receptor is represented by the SAS area. (B−D) Average structure of the refined Aurora-A/pVHL complex. The binding pocket of Aurora-A is also represented by the SAS area. The pVHL ribbon is colored in blue light, and the key residues of the binding pocket are colored in brown.

Monte Carlo minimization-conformational sampling and MD simulations were then performed to reveal how the pVHL protein binds with the Aurora-A enzyme and predict the corresponding Aurora-A/pVHL binding free energy.[74,75]

The most favorable Aurora-A/pVHL binding mode was identified using clustering of the binding conformations (Figure 6A). Molecular docking revealed few clusters of the binding modes, but only the primary cluster with the most populated conformation was associated with the expected strong binding between the pVHL^{Leu117} side-chain and the solvent exposed side-chain residues of the αC and αE helices of the Aurora-A binding pocket, and this binding mode corresponded to the lowest interaction energy. Interestingly, this residue is completely conserved in the pVHL superfamily, and equivalent hydrophobic interactions have been previously reported in pVHL−Elongin C complex structures.[45] The results consistently showed that the residues accessible to the solvent of the pVHL helix H1 fit into the binding site cavity with most conformations in close contact with the Ile184, Leu188, Val252, and Phe275 side chains of Aurora-A (Figure 6). Thus, pVHL binding with Aurora-A can be regarded as strong and specific as it reaches vdW interactions with the hydrophobic residues of the pocket.

Stability of the MD-Simulated Aurora-A/pVHL Complex. To further assess the reliability of the docked pVHL structures, the conformation with the lowest interaction energy from the major cluster was refined by MD simulation in water. To evaluate the deviation of the trajectory from the initial docked Aurora-A/pVHL structure, the Cα rms deviation of pVHL was monitored over 15 ns trajectories with rotational and translational motions removed (Figure 7). The Cα rms deviation of the full length of pVHL was quite high (between 3.0 and 4.0 Å) through

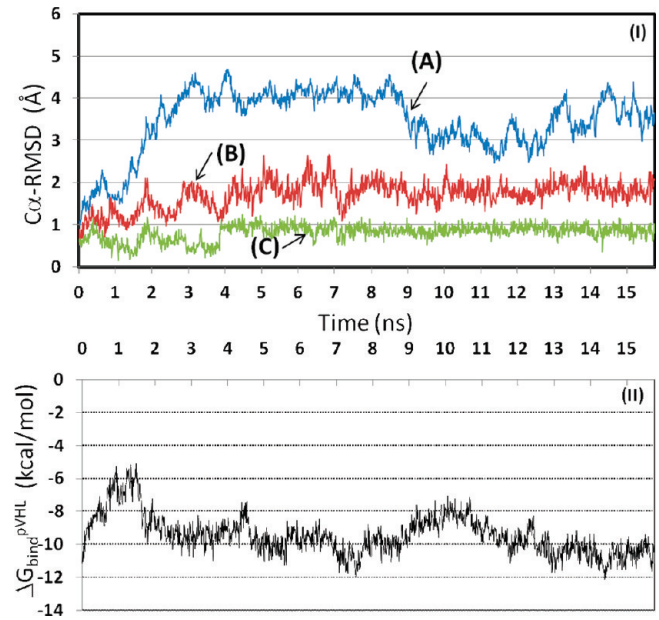

Figure 7. (I) Plot of MD-simulated Cα-rmsd of the pVHL protein versus simulation time for Aurora-A/pVHL complex. Trace A represents the Cα-rmsd of the full length of the pVHL. Trace B represents the Cα-rmsd of the pVHL loop comprising residues 107−116. Trace C represents the Cα-rmsd of the pVHL Helix H1 (residues 117−128). (II) Plot of the binding free energy (kcal/mol) of pVHL protein (ΔG_{bind}^{pVHL}) versus simulation time for the Aurora-A/pVHL complex.

the MD simulations with respect to the starting, docked Aurora-A/pVHL structure, possibly reflecting the general conformational

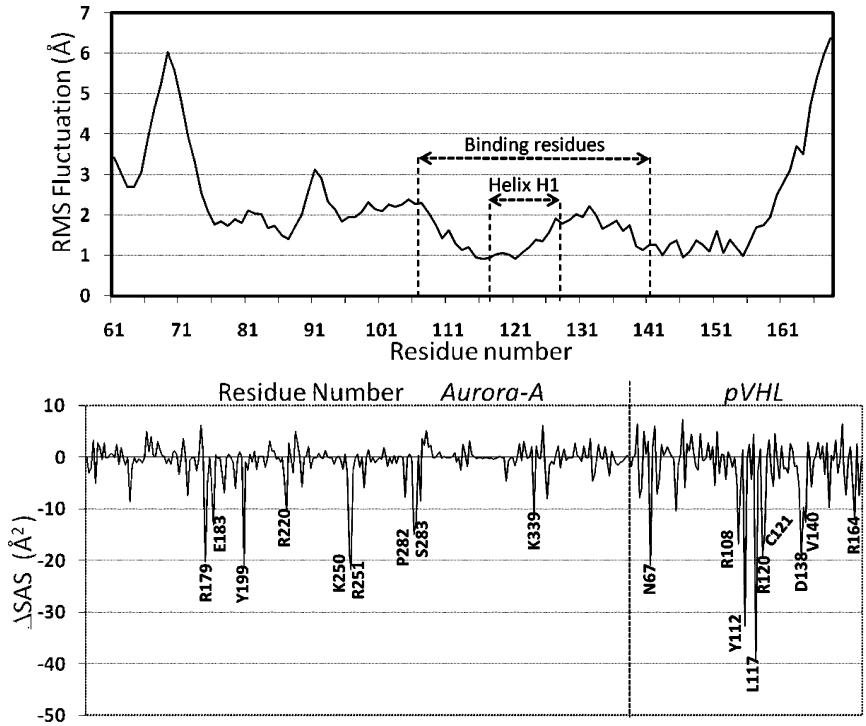

Figure 8. (top) Cα RMSF per residue for the pVHL binding with Aurora-A receptor during the MD simulation. Residue displacement calculated for each Cα atom as a function of residue number averaged over the first six eigenvectors for the MD simulations of the pVHL protein binding with Aurora-A receptor. (bottom) Difference of the solvent accessibility surface area (SAS) between the bound Aurora-A/pVHL complex and the proteins in free form, defined by ΔSAS = SAS(complex) − SAS(pVHL) − SAS(Aurora-A).

lability of the unstructured region of the pVHL protein. However, it was evident that the degree of conformational drift in the aqueous environment of the helix H1 domain and the loop (residues 107−116) interacting with Aurora-A was significantly less than the degree of drift in the whole protein. For the pVHL helix H1 domain, the MD simulation rapidly achieved stability in the Cα rms deviation with a value around 0.9 Å, whereas, for residues 107−116, the Cα rms deviation increased to ∼1.8 Å after ∼5.0 ns, thus maintaining low structural change through the next ∼10 ns. The jumps observed at ∼5 ns were due to the adoption of a more stable conformation of the pVHL protein, producing a minor change in the flexible loop of the Aurora-A binding site. Therefore, the relatively high values and the irregular profile of the plot reflected the structural changes of the highly flexible protein regions and seemed to have little or no structural effect on the pVHL binding mode with the Aurora-A active site (Figure 7).

Essential Dynamics (ED) Analysis of pVHL Protein in Aurora-A/pVHL Complex. Moreover, the rms fluctuation profiles suggest that these conformational changes are accompanied by significant changes in the local flexibility of the protein chain. Hence, it behooved us to examine the implications of this extreme plasticity of the pVHL structure upon binding to the Aurora-A receptor. Thus, the stabile and flexible regions of the pVHL binding structure were also checked by computing the atomic fluctuations through the MD trajectory. Using a stable trajectory, ED analysis was performed to examine changes in the dynamical structures of the pVHL binding with Aurora-A. ED identifies functionally relevant displacements of groups of residues and emphasizes the amplitude and direction of dominant protein motions by concentrating on a subset of the principal eigenvalues and eigenvectors of the residue pair covariance matrix calculated from MD. For the ED analysis of the pVHL MD trajectory, only a few eigenvectors were found to represent the essential motions in the protein. Figure 8 shows the displacements as a function of residue number averaged over the first six eigenvectors for the Aurora-A/pVHL MD simulation. The results of the ED analysis qualitatively confirm previous findings. Relatively large displacements occurred in the pVHL β-domain, while the binding residues of the α-domain showed smaller movements. The overall pattern of displacements shown in Figure 8 is related to the results of the above-calculated Cα rms deviation of the pVHL protein (Figure 7). The regions that contain some degree of secondary structure have low rms values, while the other regions fluctuate more, as indicated by the large rms fluctuation values. An interesting feature of the rms fluctuation plot (Figure 8) is the periodicity in the fluctuations, indicating that, while there are regions of low movement, there are also some very flexible regions. This may be necessary to keep the pVHL binding regions in contact with the residues of the Aurora-A pocket, while maintaining pVHL protein flexibility upon binding to its receptor.

Binding Free Energy $\Delta G_{bind}{}^{pVHL}$ of pVHL to Aurora-A Receptor. To ensure that the docked pVHL protein was binding efficiently to the Aurora-A active site during the solvated MD simulation, the binding Gibbs free energy $\Delta G_{bind}{}^{pVHL}$ of pVHL to Aurora-A was monitored as a function of simulation time. Figure 7 presents the binding free energy $\Delta G_{bind}{}^{pVHL}$ of the pVHL protein to the Aurora-A receptor during the 15 ns MD simulations. It is also important to monitor energy variation, in order to determine whether and when equilibration is reached. As seen in Figure 7, the binding Gibbs free energy $\Delta G_{bind}{}^{pVHL}$ remained constant after 12 ns, indicating that the 3D model of the Aurora-A/pVHL complex was structurally stable during the last 4 ns of MD simulation time. These results indicate that the initial recognition of pVHL with Aurora-A involved a few interactions between the loop residues (107−116) of pVHL and the Aurora-A binding pocket. Gradually, the interaction between

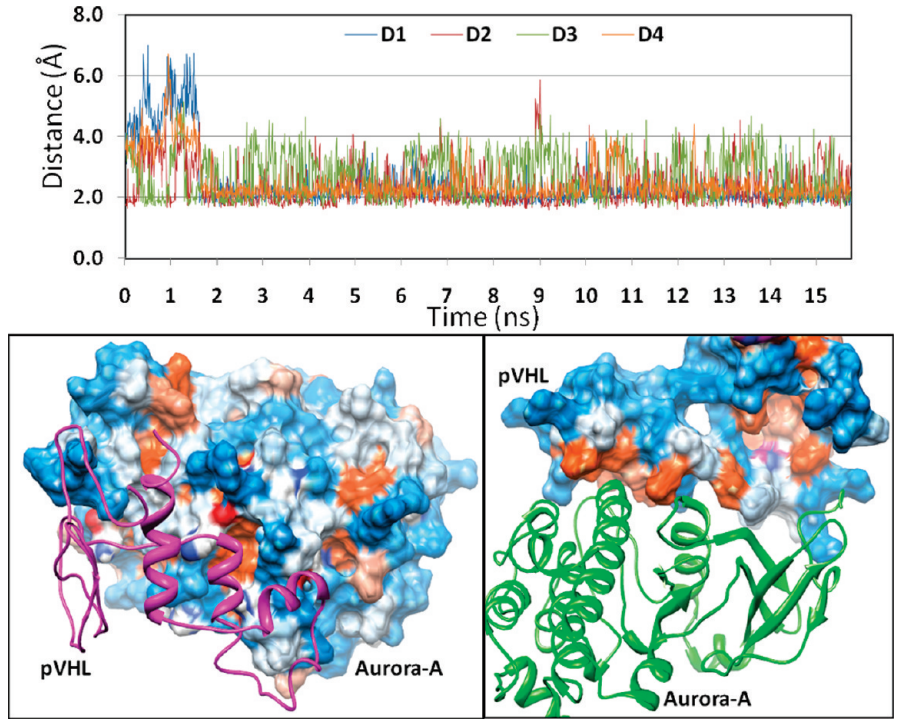

Figure 9. Plots of MD-simulated internuclear distances of the pVHL protein versus simulation time for Aurora-A/pVHL complex. Trace D1 represent the H-bond between the $His280^{H\varepsilon}$ atom of Aurora-A and carbonyl backbone $Cys121^{C=O}$ of pVHL. Traces D2 and D3 represent the bidentate H-bond distances between the oxygen and hydrogen of the $pVHL^{Arg120}$ guanidinum side chain and the carboxylate group of the $Aurora\text{-}A^{Glu183}$ residue. Trace D4 represents the H-bond between the $His187^{N\varepsilon}$ atom (see Figure SI-3 in the Supporting Information) of Aurora-A and the C═O carbonyl group of the $pVHL^{Tyr115}$ residue. The H-bonds are displayed by a red dashed line. (bottom) Solvent accessible surface area (SAS) on Aurora-A (left) and pVHL (right) proteins for the refined MD-simulated Aurora-A/pVHL complex. The SAS is colored according to the hydrophobicity of the residues. The colors range from dodger blue for the most hydrophilic residues, through white, and then to orange red for the most hydrophobic residues.

the proteins occurred and was enhanced by the conformational changes of the pVHL loop. The Gibbs free energy ($\Delta G_{bind}{}^{pVHL}$) of pVHL binding to Aurora-A was estimated for the last 1 ns of the simulations (see Materials and Methods), yielding an average value of −10.55 kcal/mol. This further indicates that the pVHL protein binds to the Aurora-A receptor with high affinity and cannot be neglected (the $\Delta G_{bind}{}^{pVHL}$ values correspond to nanomolar pVHL affinities).

pVHL Protein Binding with Aurora-A Enzyme. The energy-minimized average Aurora-A/pVHL structure obtained from the MD simulation is shown in Figures 6 and 9. The docking study of the complex reveals that the helix H1 of the pVHL α-domain fits into the concave surface of Aurora-A, inserting hydrophobic side-chains into the pocket along the surface. Reciprocally, the helix αE of Aurora-A, which bulges out from the side of the concave surface, fits into an extended groove formed by the H1, H2, and H3 helices of the pVHL α-domain and completes the intermolecular four-helix cluster packing (Figure 6). The most significant vdW contacts are made by the $pVHL^{Leu117}$ side-chain, which protrudes from the helix H1 and fits into the large hydrophobic pocket in the binding groove at the intersection of the αC and αE helices of the Aurora-A enzyme and forms hydrophobic interactions with the Ile184, His187, Leu188, Tyr246, Lys250 (with alkyl chain), and Val252 side-chains. Additional contacts are made by the loop (residues 107−116) of the pVHL binding α-domain with the receptor through several H-bonds and long-range electrostatic interactions.

Hence, the His187 and His280 side-chains of Aurora-A and the NH backbone atoms of $pVHL^{Tyr115}$ and the C═O carbonyl group of $pVHL^{Cys121}$ occupy positions suitable for the formation of favorable H-bonds. The fluctuation of these H-bonds is described by the distances D1 and D4 in Figure 9. In addition to these H-bonds, the interaction of pVHL helix H1 with the Aurora-A pocket is enhanced by the formation of a bidentate salt bridge between the $pVHL^{Arg120}$ and $Aurora\text{-}A^{Glu183}$ side-chains (Figure 9). Figure SI-3 in the Supporting Information demonstrates the most important hydrogen bonds between the pVHL helix H1 and the Aurora-A binding pocket in our MD simulations. Furthermore, the residues Val114, Val124, and Leu143 of pVHL also appear to be important hydrophobic binding-site residues for the model. The Aurora-A/pVHL complex model shows that the basic pVHL surface (Figure SI-4 in the Supporting Information) complements the acidic Aurora-A surface, but only a few salt bridges are observed.

As a final point, the loss in solvent-accessible surface (ΔSAS) area was calculated for each residue in the Aurora-A/pVHL complex and the protein free form. The residues with loss more than 40% in SAS area upon the formation of the Aurora-A/pVHL complex are displayed in Figure 8. These residues were selected as the potential binding sites. Together with the interaction information of hydrogen bonds, van der Waals contacts and electrostatic interactions between pVHL and Aurora-A, the residues that are most likely to be involved in interaction between pVHL and Aurora-A in the complex were obtained (Figures 6 and 8). Furthermore, the solvent-accessible surface area (ΔSAS) excluded upon interaction is 189 $Å^2$ from Aurora-A and 238 $Å^2$ from pVHL, which come mainly from the helix H1 in pVHL, and the region near and within the αC and αE helices of the Aurora-A pocket. The most significant loss in SAS area in our simulated Aurora-A/pVHL complex appears to be consistent with those described for the binding of TPX2 with Aurora-A protein.[53]

Conclusion

The Aurora-A enzyme is overexpressed in several human cancers and plays a critical role in centrosome maturation and separation, thereby regulating spindle assembly and stability during mitosis. The role of this protein in oncogenic transformation and progression occurs because Aurora-A is coregulated with P53 and the silencing of Aurora-A results in less phosphorylation and more stability of p53 leading to cell-cycle arrest at G2-M. The cellular functions of Aurora-A are also mediated via a number of proteins involved in mitosis. Notably, a cellular component, the target protein of XKlp2 (TPX2), has been shown to be an important binding partner and regulator of Aurora-A. TPX2 binding not only prevents the inactivation of Aurora-A but also increases the kinase activity of the activated Aurora-A protein.

In this study, a multidisciplinary approach that combines experimental data, docking, MD simulations, and binding free energy methods has been used to investigate the interactions of pVHL with Aurora-A. The preliminary results of biological assays presented evidence that pVHL binds strongly to Aurora-A. To provide molecular explanations of the *in vitro* observations, we analyzed in detail the binding mode and dynamic behavior of pVHL protein with Aurora-A enzyme, in an effort to identify the key residues involved in the assembly of the complex. The molecular docking study of the Aurora-A/TPX2 complex showed that pVHL helix H1 fits and stabilizes into the hydrophobic cavity of Aurora-A in a similar fashion to that observed in the Aurora-A/TPX2 crystal structure. Indeed, the crystal structure of the Aurora-A/TPX2 complex shows that TPX2 makes two contacts with the Aurora-A kinase domain. The interactions between TPX2 and Aurora-A help mold the activation loop into a conformation that is ready for substrate binding. Similarly, we demonstrated that pVHL may be a physiologically important binding partner of Aurora-A and should regulate the enzyme activity by increasing the affinity of ATP.

The agreement between our Aurora-A/pVHL complex model, as well as experimentally determined structures of Aurora-A/TPX2 and pVHL-Elongin C−Elongin B complexes, highly supports the fact that the quality of our complex model is adequate for further experimental investigations of the interfaces identified for the Aurora-A/pVHL complex.

It is well-known that the conformational flexibility of proteins often prevents accurate ligand binding affinity prediction and rational inhibitor design. Comparisons of the Aurora-A/TPX2/ADP and Aurora-A/inhibitor structures suggest that, to allow ligands to bind to the back pocket (inhibitor active site), the C helix needs to shift up and out. This conformational change is more restricted when pVHL (or TPX2) is bound due to the interactions between pVHL and the C helix. Thus, to design novel ATP competitors that show specificity for the inhibition of Aurora-A, our hypothesis is that pVHL binding reduces the flexibility of back-pocket-binding inhibitors by restricting the conformational changes of the active site residues. As a result, the current computational study of the Aurora-A/pVHL complex could provide the rationale for the development of the next generation of anticancer drugs with improvements in affinity and selectivity profiles against Aurora-A kinase.

Acknowledgment. The research was supported in part by Tunisian State Secretariat for Research and Technology and by UNDP/World Bank/WHO (Grant No. 990960 to A.H.).

Supporting Information Available: Four figures concerning more detailed information about the homology modeling and MD-simulated structures of Aurora-A/pVHL complex. This material is available free of charge via the Internet at http://pubs.acs.org.

References and Notes

(1) Meraldi, P.; Honda, R.; Nigg, E. A. Aurora kinases link chromosome segregation and cell division to cancer susceptibility. *Curr. Opin. Genet. Dev.* **2004**, *14*, 29–36.

(2) Sakakura, C.; Hagiwara, A.; Yasuoka, R.; Fujita, Y.; Nakanishi, M.; Masuda, K.; Shimomura, K.; Nakamura, Y.; Inazawa, J.; Abe, T.; Yamagishi, H. Tumour-amplified kinase BTAK is amplified and overexpressed in gastric cancers with possible involvement in aneuploid formation. *Br. J. Cancer* **2001**, *84*, 824–831.

(3) Zhu, J. J.; Abbruzzese, J. L.; Izzo, J.; Hittelman, W. N.; Li, D. H. AURKA amplification, chromosome instability, and centrosome abnormality in human pancreatic carcinoma cells. *Cancer Genet. Cytogenet.* **2005**, *159*, 10–17.

(4) Marumoto, T.; Zhang, D. W.; Saya, H. Aurora-A - A guardian of poles. *Nat. Rev. Cancer* **2005**, *5*, 42–50.

(5) Warner, S. L.; Bearss, D. J.; Han, H. Y.; Von Hoff, D. D. Targeting aurora-2 kinase in cancer. *Mol. Cancer Ther.* **2003**, *2*, 589–595.

(6) Keen, N.; Taylor, S. Aurora-kinase inhibitors as anticancer agents. *Nat. Rev. Cancer* **2004**, *4*, 927–936.

(7) Bird, A. W.; Hyman, A. A. Building a spindle of the correct length in human cells requires the interaction between TPX2 and Aurora A. *J. Cell Biol.* **2008**, *182*, 289–300.

(8) Pugacheva, E. N.; Golemis, E. A. The focal adhesion scaffolding protein HEF1 regulates activation of the Aurora-A and Nek2 kinases at the centrosome. *Nat. Cell Biol.* **2005**, *7*, 937–U18.

(9) Hutterer, A.; Berdnik, D.; Wirtz-Peitz, F.; Zigman, M.; Schleiffer, A.; Knoblich, J. A. Mitotic activation of the kinase Aurora-A requires its binding partner Bora. *Dev. Cell* **2006**, *11*, 147–157.

(10) Eyers, P. A.; Erikson, E.; Chen, L. G.; Maller, J. L. A novel mechanism for activation of the protein kinase aurora A. *Curr. Biol.* **2003**, *13*, 691–697.

(11) Harrington, E. A.; Bebbington, D.; Moore, J.; Rasmussen, R. K.; Ajose-Adeogun, A. O.; Nakayama, T.; Graham, J. A.; Demur, C.; Hercend, T.; Diu-Hercend, A.; Su, M.; Golec, J. M. C.; Miller, K. M. VX-680, a potent and selective small-molecule inhibitor of the Aurora kinases, suppresses tumor growth in vivo. *Nat. Med.* **2004**, *10*, 262–267.

(12) Hoar, K.; Chakravarty, A.; Rabino, C.; Wysong, D.; Bowman, D.; Roy, N.; Ecsedy, J. A. MLN8054, a small-molecule inhibitor of Aurora A, causes spindle pole and chromosome congression defects leading to aneuploidy. *Mol. Cell Biol.* **2007**, *27*, 4513–4525.

(13) Zhang, Z. H.; Singh, M.; Davidson, S.; Rosen, D. G.; Yang, G.; Liu, J. S. Activation of BTAK expression in primary ovarian surface epithelial cells of prophylactic ovaries. *Mod. Pathol.* **2007**, *20*, 1078–1084.

(14) Nadler, Y.; Camp, R. L.; Schwartz, C.; Rimm, D. L.; Kluger, H. M.; Kluger, Y. Expression of Aurora a (but not Aurora B) is predictive of survival in breast cancer. *Clin. Cancer Res.* **2008**, *14*, 4455–4462.

(15) Ogawa, E.; Takenaka, K.; Katakura, H.; Adachi, M.; Otake, Y.; Toda, Y.; Kotani, H.; Manabe, T.; Wada, H.; Tanaka, F. Perimembrane Aurora-A expression is a significant prognostic factor in correlation with proliferative activity in non-small-cell lung cancer (NSCLC). *Ann. Surg. Oncol.* **2008**, *15*, 547–554.

(16) Comperat, E.; Bieche, I.; Dargere, D.; Laurendeau, I.; Vielliefond, A.; Benoit, G.; Vidaud, M.; Camparo, P.; Capron, F.; Verret, C.; Cussenot, O.; Bedossa, P.; Paradis, V. Gene expression study of Aurora-A reveals implication during bladder carcinogenesis and increasing values in invasive urothelial cancer. *Urology* **2008**, *72*, 873–877.

(17) Agnese, V.; Cabibi, D.; Calcara, D.; Terrasi, M.; Pantuso, G.; Fiorentino, E.; Intrivici, C.; Colucci, G.; Aragona, F.; Gebbia, N.; Bazan, V. Russo, A. *Aurora-A overexpression as an early marker of reflux-related columnar mucosa and Barrett's oesophagus. Ann. Oncol.* **2007**, *18*, 110−115.

(18) Rojanala, S.; Han, H. Y.; Munoz, R. M.; Browne, W.; Nagle, R.; Von Hoff, D. D.; Bearss, D. J. The mitotic serine threonine kinase, Aurora-2, is a potential target for drug development in human pancreatic cancer. *Mol. Cancer Ther.* **2004**, *3*, 451–457.

(19) Wiseman, S. M.; Melck, A.; Masoudi, H.; Ghaidi, F.; Goldstein, L.; Gown, A.; Jones, S. J. M.; Griffith, O. L. Molecular phenotyping of thyroid tumors identifies a marker panel for differentiated thyroid cancer diagnosis. *Ann. Surg. Oncol.* **2008**, *15*, 2811–2826.

(20) Ehara, H.; Yokoi, S.; Tamaki, M.; Nishino, Y.; Takahashi, Y.; Deguchi, T.; Kimura, M.; Yoshioka, T.; Okano, Y. Expression of mitotic Aurora/Ipl1p-related kinases in renal cell carcinomas: an immunohistochemical study. *Urol. Res.* **2003**, *31*, 382–386.

(21) Kurahashi, T.; Miyake, H.; Hara, I.; Fujisawa, M. Significance of Aurora-A expression in renal cell carcinoma. *Urol. Oncol.: Semin. Orig. Invest.* **2007**, *25*, 128–133.

(22) Banks, R. E.; Tirukonda, P.; Taylor, C.; Hornigold, N.; Astuti, D.; Cohen, D.; Maher, E. R.; Stanley, A. J.; Harnden, P.; Joyce, A.; Knowles,

M.; Selby, P. J. Genetic and epigenetic analysis of von Hippel-Lindau (VHL) gene alterations and relationship with clinical variables in sporadic renal cancer. *Cancer Res.* **2006**, *66*, 2000–2011.

(23) Brauch, H.; Weirich, G.; Brieger, J.; Glavac, D.; Rodl, H.; Eichinger, M.; Feurer, M.; Weidt, E.; Puranakanitstha, C.; Neuhaus, C.; Pomer, S.; Brenner, W.; Schirmacher, P.; Storkel, S.; Rotter, M.; Masera, A.; Gugeler, N.; Decker, H. J. VHL alterations in human clear cell renal cell carcinoma: Association with advanced tumor stage and a novel hot spot mutation. *Cancer Res.* **2000**, *60*, 1942–1948.

(24) Kim, W. Y.; Kaelin, W. G. Role of VHL gene mutation in human cancer. *J. Clin. Oncol.* **2004**, *22*, 4991–5004.

(25) Lolkema, M. P.; Gervais, M. L.; Snijckers, C. M.; Hill, R. P.; Giles, R. H.; Voest, E. E.; Ohh, M. Tumor suppression by the von hippel-lindau protein requires phosphorylation of the acidic domain. *J. Biol. Chem.* **2005**, *280*, 22205–22211.

(26) Schoenfeld, A.; Davidowitz, E. J.; Burk, R. D. A second major native von Hippel-Lindau gene product, initiated from an internal translation start site, functions as a tumor suppressor. *Proc. Natl. Acad. Sci. U.S.A.* **1998**, *95*, 8817–8822.

(27) Pause, A.; Lee, S.; Lonergan, K. M.; Klausner, R. D. The von Hippel-Lindau tumor suppressor gene is required for cell cycle exit upon serum withdrawal. *Proc. Natl. Acad. Sci. U.S.A.* **1998**, *95*, 993–998.

(28) Kim, M.; Katayose, Y.; Li, Q. D.; Rakkar, A. N. S.; Li, Z. W.; Hwang, S. G.; Katayose, D.; Trepel, J.; Cowan, K. H.; Seth, P. Recombinant adenovirus expressing Von Hippel-Lindau-mediated cell cycle arrest is associated with the induction of cyclin-dependent kinase inhibitor p27(Kip1). *Biochem. Biophys. Res. Commun.* **1998**, *253*, 672–677.

(29) Davidowitz, E. J.; Schoenfeld, A. R.; Burk, R. D. VHL induces renal cell differentiation and growth arrest through integration of cell-cell and cell-extracellular matrix signaling. *Mol. Cell Biol.* **2001**, *21*, 865–874.

(30) Hergovich, A.; Lisztwan, J.; Barry, R.; Ballschmieter, P.; Krek, W. Regulation of microtubule stability by the von Hippel-Lindau tumour suppressor protein pVHL. *Nat. Cell Biol.* **2003**, *5*, 64–70.

(31) Lolkema, M. P.; Mehra, N.; Jorna, A. S.; van Beest, M.; Giles, R. H.; Voest, E. E. The von Hippel-Lindau tumor suppressor protein influences microtubule dynamics at the cell periphery. *Exp. Cell Res.* **2004**, *301*, 139–146.

(32) Kuehn, E. W.; Walz, G.; Benzing, T. von Hippel-Lindau: A tumor suppressor links Microtubules to ciliogenesis and cancer development. *Cancer Res.* **2007**, *67*, 4537–4540.

(33) Mack, F. A.; Rathmell, W. K.; Arsham, A. M.; Gnarra, J.; Keith, B.; Simon, M. C. Loss of pVHL is sufficient to cause HIF dysregulation in primary cells but does not promote tumor growth. *Cancer Cell* **2003**, *3*, 75–88.

(34) Frew, I. J.; Krek, W. Multitasking by pVHL in tumour suppression. *Curr. Opin. Cell Biol.* **2007**, *19*, 685–690.

(35) Maynard, M. A.; Ohh, M. von Hippel-Lindau tumor suppressor protein and hypoxia-inducible factor in kidney cancer. *Am. J. Nephrol.* **2004**, *24*, 1–13.

(36) Chen, F. K. T.; Yao, M.; Hustad, T.; Glavac, D.; Dean, M.; Gnarra, J. R.; Orcutt, M. L.; Duh, F. M.; Glenn, G. Germline mutations in the von Hippel-Lindau disease tumor suppressor gene: correlations with phenotype. *Hum. Mutat.* **1995**, *5*, 66–75.

(37) Gallou, C.; Joly, D.; Mejean, A.; Staroz, F.; Martin, N.; Tarlet, G.; Orfanelli, M. T.; Bouvier, R.; Droz, D.; Chretien, Y.; Marechal, J. M.; Richard, S.; Junien, D.; Beroud, C. Mutations of the VHL gene in sporadic renal cell carcinoma: Definition of a risk factor for VHL patients to develop an RCC. *Hum. Mutat.* **1999**, *13*, 464–475.

(38) Wiesener, M. S.; Seyfarth, M.; Warnecke, C.; Jurgensen, J. S.; Rosenberger, C.; Morgan, N. V.; Maher, E. R.; Frei, U.; Eckardt, K. U. Paraneoplastic erythrocytosis associated with an inactivating point mutation of the von Hippel-Lindau gene in a renal cell carcinoma. *Blood* **2002**, *99*, 3562–3565.

(39) Tsai, M. Y.; Zheng, Y. X. Aurora A kinase-coated beads function as microtubule-organizing centers and enhance RanGTP-induced spindle assembly. *Curr. Biol.* **2005**, *15*, 2156–2163.

(40) Castro, A.; Arlot-Bonnemains, Y.; Vigneron, S.; Labbe, J. C.; Prigent, C.; Lorca, T. APC/Fizzy-Related targets Aurora-A kinase for proteolysis. *EMBO Rep.* **2002**, *3*, 457–462.

(41) Bradford, M. M. Rapid and sensitive method for quantitation of microgram quantities of protein utilizing principle of protein-dye binding. *Anal. Biochem.* **1976**, *72*, 248–254.

(42) Benson, D. A.; Boguski, M. S.; Lipman, D. J.; Ostell, J.; Ouellette, B. F. F.; Rapp, B. A.; Wheeler, D. L. GenBank. *Nucleic Acids Res.* **1999**, *27*, 12–17.

(43) Altschul, S. F.; Gish, W.; Miller, W.; Myers, E. W.; Lipman, D. J. BASIC LOCAL ALIGNMENT SEARCH TOOL. *J. Mol. Biol.* **1990**, *215*, 403–410.

(44) Berman, H. M.; Westbrook, J.; Feng, Z.; Gilliland, G.; Bhat, T. N.; Weissig, H.; Shindyalov, I. N.; Bourne, P. E. The Protein Data Bank. *Nucleic Acids Res.* **2000**, *28*, 235–242.

(45) Stebbins, C. E.; Kaelin, W. G.; Pavletich, N. P. Structure of the VHL-ElonginC-ElonginB complex: Implications for VHL tumor suppressor function. *Science* **1999**, *284*, 455–461.

(46) Schwede, T.; Kopp, J.; Guex, N.; Peitsch, M. C. SWISS-MODEL: an automated protein homology-modeling server. *Nucleic Acids Res.* **2003**, *31*, 3381–3385.

(47) Guex, N.; Peitsch, M. C. Swiss-Model and the Swiss-PdbViewer: an environment for comparative protein modelling. *Electrophoresis* **1997**, *18*, 2714–2723.

(48) Gunsteren, W. F. v.; Billeter, S. R.; Eising, A. A.; Hünenberger, P. H.; Krüger, P.; Mark, A. E.; Scott, W. R. P. Tironi, I. G. *Biomolecular simulations: GROMOS96 Manual and User Guide*; VdF: Hochschulverlag AG an der ETH Zürich and BIOMOS b.v, Zürich, Groningen, 1996; ISBN 3 7281 2422 2.

(49) Hooft, R.W. W.; Sander, C.; Vriend, G. Verification of protein structures: Side-chain planarity. *J. Appl. Crystallogr.* **1996**, *29*, 714–716.

(50) Sippl, M. J. Recognition of errors in three-dimensional structures of proteins. *Proteins* **1993**, *17*, 355–362.

(51) Melo, F.; Feytmans, E. Assessing protein structures with a non-local atomic interaction energy. *J. Mol. Biol.* **1998**, *277*, 1141–1152.

(52) Eisenberg, D.; Luthy, R. Bowie, J. U. VERIFY3D: Assessment of protein models with three-dimensional profiles. *Macromol. Crystallogr., Part B* **1997**, *277*, 396−404.

(53) Bayliss, R.; Sardon, T.; Vernos, I.; Conti, E. Structural basis of Aurora-A activation by TPX2 at the mitotic spindle. *Mol. Cell* **2003**, *12*, 851–862.

(54) Harvey, S. C. Treatment of electrostatic effects in macromolecular modeling. *Proteins: Struct., Funct., Genet.* **1989**, *5*, 78–92.

(55) Guenot, J.; Kollman, P. A. Molecular dynamics studies of a DNA-binding protein: 2. An evaluation of implicit and explicit solvent models for the molecular dynamics simulation of the Escherichia coli trp repressor. *Protein Sci.* **1992**, *1*, 1185–1205.

(56) Gatchell, D. W.; Dennis, S.; Vajda, S. Discrimination of near-native protein structures from misfolded models by empirical free energy functions. *Proteins: Struct., Funct., Genet.* **2000**, *41*, 518–534.

(57) Kozakov, D.; Clodfelter, K. H.; Vajda, S.; Camacho, C. J. Optimal clustering for detecting near-native conformations in protein docking. *Biophys. J.* **2005**, *89*, 867–875.

(58) Lindahl, E.; Hess, B.; van der Spoel, D. GROMACS 3.0: a package for molecular simulation and trajectory analysis. *J. Mol. Model.* **2001**, *7*, 306–317.

(59) Schuler, L. D.; Daura, X.; Van Gunsteren, W. F. An improved GROMOS96 force field for aliphatic hydrocarbons in the condensed phase. *J. Comput. Chem.* **2001**, *22*, 1205–1218.

(60) Bargagna-Mohan, P.; Hamza, A.; Kim, Y. E.; Ho, Y. K. A.; Mor-Valknin, N.; Wendschlag, N.; Li, J. J.; Evans, R. M.; Markovitz, D. M.; Zhan, C. G.; Kim, K. B.; Mohan, R. The tumor inhibitor and antiangiogenic agent withaferin A targets the intermediate filament protein vimentin. *Chem. Biol.* **2007**, *14*, 623–634.

(61) Choa, H.; Huang, L. Y.; Hamza, A.; Gao, D. Q.; Zhan, C. G.; Tai, H. H. Role of glutamine 148 of human 15-hydroxyprostaglandin dehydrogenase in catalytic oxidation of prostaglandin E-2. *Bioorg. Med. Chem.* **2006**, *14*, 6486–6491.

(62) Zhang, T.; Hamza, A.; Cao, X. H.; Wang, B.; Yu, S. W.; Zhan, C. G.; Sun, D. X. A novel Hsp90 inhibitor to disrupt Hsp90/Cdc37 complex against pancreatic cancer cells. *Mol. Cancer Ther.* **2008**, *7*, 162–170.

(63) Berendsen, H. J. C.; Postma, J. P. M.; van Gunsteren, W. F. Hermans, J. In *Intermolecular Forces*; Pullman, B., Ed.; D. Reidel Publishing Co.: Dordrecht, The Netherlands, 1981; pp 331−342.

(64) Essmann, U.; Perera, L.; Berkowitz, M. L.; Darden, T.; Lee, H.; Pedersen, L. G. A smooth particle mesh ewald method. *J. Chem. Phys.* **1995**, *103*, 8577–8593.

(65) Berendsen, H. J. C.; Postma, J. P. M.; Vangunsteren, W. F.; Dinola, A.; Haak, J. R. Molecular-dynamics with coupling to an external bath. *J. Chem. Phys.* **1984**, *81*, 3684–3690.

(66) Hess, B.; Bekker, H.; Berendsen, H. J. C.; Fraaije, J. LINCS: A linear constraint solver for molecular simulations. *J. Comput. Chem.* **1997**, *18*, 1463–1472.

(67) Naim, M.; Bhat, S.; Rankin, K. N.; Dennis, S.; Chowdhury, S. F.; Siddiqi, I.; Drabik, P.; Sulea, T.; Bayly, C. I.; Jakalian, A.; Purisima, E. O. Solvated interaction energy (SIE) for scoring protein-ligand binding affinities. 1. Exploring the parameter space. *J. Chem. Inf. Model.* **2007**, *47*, 122–133.

(68) Cui, Q. Z.; Sulea, T.; Schrag, J. D.; Munger, C.; Hung, M. N.; Naim, M.; Cygler, M.; Purisima, E. O. Molecular dynamics-solvated interaction energy studies of protein-protein interactions: The MP1-p14 scaffolding complex. *J. Mol. Biol.* **2008**, *379*, 787–802.

(69) Amadei, A.; Linssen, A. B. M.; Berendsen, H. J. C. Essential dynamics of proteins. *Proteins: Struct., Funct., Genet.* **1993**, *17*, 412–425.

(70) Capozzi, F.; Luchinat, C.; Micheletti, C.; Pontiggia, F. Essential dynamics of helices provide a functional classification of EF-hand proteins. *J. Proteome Res.* **2007**, *6*, 4245–4255.

(71) Stepanova, M. Dynamics of essential collective motions in proteins: Theory. *Phys. Rev. E* **2007**, 76.

(72) Kaelin, W. G. Molecular basis of the VHL hereditary cancer syndrome. *Nat. Rev. Cancer* **2002**, *2*, 673–682.

(73) Ohh, M.; Takagi, Y.; Aso, T.; Stebbins, C. E.; Pavletich, N. P.; Zbar, B.; Conaway, R. C.; Conaway, J. W.; Kaelin, W. G. Synthetic peptides define critical contacts between elongin C, elongin B, and the von Hippel-Lindau protein. *J. Clin. Invest.* **1999**, *104*, 1583–1591.

(74) Li, Z. Q.; Scheraga, H. A. Monte-carlo-minimization approach to the multiple-minima problem in protein folding. *Proc. Natl. Acad. Sci. U.S.A.* **1987**, *84*, 6611–6615.

(75) Rangarajan, E. S.; Ruane, K. M.; Sulea, T.; Watson, D. C.; Proteau, A.; Leclerc, S.; Cygler, M.; Matte, A.; Young, N. M. Structure and active site residues of Pg1D, an N-acetyltransferase from the Bacillosamine synthetic pathway required for N-glycan synthesis in Campylobacter jejuni. *Biochemistry* **2008**, *47*, 1827–1836.

JP909869G